

Article

Atomic Layer Deposition of Ultrathin $\text{La}_2\text{O}_3/\text{Al}_2\text{O}_3$ Nanolaminates on MoS_2 with Ultraviolet Ozone Treatment

Jibin Fan ^{1,*}, Yimeng Shi ¹, Hongxia Liu ², Shulong Wang ², Lijun Luan ¹, Li Duan ¹, Yan Zhang ¹ and Xing Wei ¹

¹ School of Materials Science and Engineering, Chang'an University, Xi'an 710061, China; 2019131040@chd.edu.cn (Y.S.); lijunl@chd.edu.cn (L.L.); liduan@chd.edu.cn (L.D.); yan.zhang@chd.edu.cn (Y.Z.); weixing_b319@163.com (X.W.)

² Key Laboratory of Wide Band-Gap Semiconductor Materials and Devices, School of Microelectronics, Xidian University, Xi'an 710071, China; hxliu@mail.xidian.edu.cn (H.L.); slwang@xidian.edu.cn (S.W.)

* Correspondence: jbfan@chd.edu.cn

Abstract: Due to the chemically inert surface of MoS_2 , uniform deposition of ultrathin high- κ dielectric using atomic layer deposition (ALD) is difficult. However, this is crucial for the fabrication of field-effect transistors (FETs). In this work, the atomic layer deposition growth of sub-5 nm $\text{La}_2\text{O}_3/\text{Al}_2\text{O}_3$ nanolaminates on MoS_2 using different oxidants (H_2O and O_3) was investigated. To improve the deposition, the effects of ultraviolet ozone treatment on MoS_2 surface are also evaluated. It is found that the physical properties and electrical characteristics of $\text{La}_2\text{O}_3/\text{Al}_2\text{O}_3$ nanolaminates change greatly for different oxidants and treatment processes. These changes are found to be associated with the residual of metal carbide caused by the insufficient interface reactions. Ultraviolet ozone pretreatment can substantially improve the initial growth of sub-5 nm H_2O -based or O_3 -based $\text{La}_2\text{O}_3/\text{Al}_2\text{O}_3$ nanolaminates, resulting in a reduction of residual metal carbide. All results indicate that O_3 -based $\text{La}_2\text{O}_3/\text{Al}_2\text{O}_3$ nanolaminates on MoS_2 with ultraviolet ozone treatment yielded good electrical performance with low leakage current and no leakage dot, revealing a straightforward approach for realizing sub-5 nm uniform $\text{La}_2\text{O}_3/\text{Al}_2\text{O}_3$ nanolaminates on MoS_2 .

Keywords: atomic layer deposition; MoS_2 ; $\text{La}_2\text{O}_3/\text{Al}_2\text{O}_3$; ultraviolet ozone



Citation: Fan, J.; Shi, Y.; Liu, H.; Wang, S.; Luan, L.; Duan, L.; Zhang, Y.; Wei, X. Atomic Layer Deposition of Ultrathin $\text{La}_2\text{O}_3/\text{Al}_2\text{O}_3$ Nanolaminates on MoS_2 with Ultraviolet Ozone Treatment. *Materials* **2022**, *15*, 1794. <https://doi.org/10.3390/ma15051794>

Academic Editor: Alexander A. Lebedev

Received: 25 January 2022

Accepted: 25 February 2022

Published: 27 February 2022

Publisher's Note: MDPI stays neutral with regard to jurisdictional claims in published maps and institutional affiliations.



Copyright: © 2022 by the authors. Licensee MDPI, Basel, Switzerland. This article is an open access article distributed under the terms and conditions of the Creative Commons Attribution (CC BY) license (<https://creativecommons.org/licenses/by/4.0/>).

1. Introduction

Silicon complementary metal-oxide-semiconductor (CMOS) devices continuing shrink in size, and keeping the generation of heat low has becoming extremely challenging [1,2]. One promising alternative approach is to use transition metal dichalcogenides (TMDs) due to their extraordinary electronic and mechanical properties [3,4]. Particularly, molybdenum disulfide (MoS_2) with a natural bandgap (1.2~1.8 eV) has attracted plenty of researches for its promising application in scaled low-power field effect transistors (FETs) and flexible devices [5,6]. A crucial step in the manufacturing of FETs is the growth of ultrathin and uniform high-k gate dielectric on MoS_2 . The mobility of MoS_2 can be further improved after high-k gate films deposition through the suppression of Coulomb scattering by the dielectric mismatch effect between the MoS_2 and high-k dielectric [7,8]. The most controlled approach for obtaining nanoscale, high-quality growth of dielectrics is atomic layer deposition (ALD). However, atomic layer deposition of ultrathin and uniform high-k gate films on MoS_2 still represents one of the key challenges to be addressed due to the lack of dangling bonds or nucleation sites on the MoS_2 surface. The physical adsorption of precursors on the surface is considered to be a key element that enables the initial ALD reaction to take place [9]. Nevertheless, the weakly physical adsorption of precursors can be easily desorbed from the surface by the subsequent purge gas [10]. The dielectric films easy to form pinhole-like defects when it is directly deposited on MoS_2 due to random nucleation at defects, edges, and impurities, especially the thickness of the dielectric less than a few nanometers [11].

However, to meet the demand of ultra-scaled FETs, the thickness of gate dielectric layer needs to be extremely thin (<5 nm) for sufficient electrostatic coupling of the gate to the semiconducting channel [12].

To cope with these challenges, the pretreatment of a MoS₂ surface with oxygen plasma [13], introduction of an additional seeding layer [14], ultraviolet ozone (UV-O₃) [15], water plasma treatment [16] have been demonstrated. Growth of sub-5 nm uniform Al₂O₃ film on MoS₂ has been achieved [12]. La₂O₃ has a high dielectric constant (~26), large band gap (~5.8 eV), and the drawback of moisture absorption can be greatly improved by mixed with a less hygroscopic oxide Al₂O₃ [17,18]. It has been studied as the candidate gate dielectric in the sub-22 nm technical process node. The La₂O₃/Al₂O₃ nanolaminate processed film can provide a higher dielectric constant and better leakage current control at the same physical thickness compared to the Al₂O₃ film. However, to date, the growth of La-based binary or ternary compounds on MoS₂ has not been investigated. Therefore, in this paper, the ALD deposition of sub-5 nm La₂O₃/Al₂O₃ nanolaminates on MoS₂ is carried out and the properties of La₂O₃/Al₂O₃ nanolaminates on MoS₂ are investigated.

2. Materials and Methods

In the experiment, n-type silicon (100) wafers with a resistivity of 2–4 Ω·cm were cleaned by RCA method and a 60 s dip in diluted HF solution was used to remove the native oxide, followed by 5 min of washing with deionized water. Then, the silicon wafers were immediately transferred to an ultra-high vacuum RF magnetron sputtering system chamber and a MoS₂ target was cleaned in 10 min by pre-sputtering under the deposition conditions. Afterward, few layers MoS₂ film was directly deposited by RF magnetron sputtering system with the RF power of 50 W at 400 °C. For sulfur compensation and defects reduction, all wafers were annealed in the hydrogen sulfide at 700 °C for 60 min. After that, some wafers were treated by UV ozone ProCleaner plus system under the power of 11.04 mW·m⁻² for 5 min at the room temperature to improve the surface of MoS₂. The Raman spectra of MoS₂ before and after UV-O₃ treatment is shown in Figure 1. The two characteristics Raman modes (A_{1g} and E_{2g}¹) of the MoS₂ can be observed and their positions changed negligibly before and after UV-O₃ treatment. It indicates that the treatment causes minimal structural damage in MoS₂. Moreover, the difference between these two peaks is 27.3 cm⁻¹, which indicated that the thickness of MoS₂ is between five and seven layers [19].

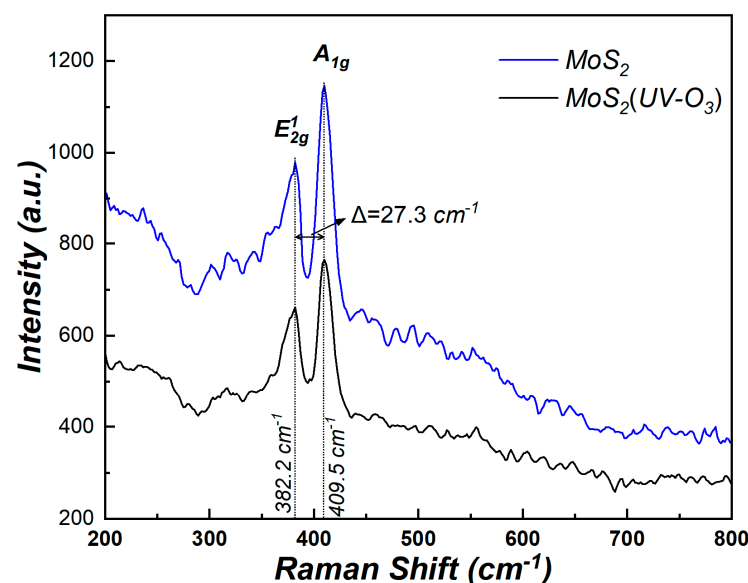


Figure 1. Raman spectra of MoS₂ before and after UV-O₃ treatment.

Then, the wafers with or without UV-O₃ treatment were transferred to the ALD chamber to deposited La₂O₃/Al₂O₃ nanolaminates at 260 °C. Tris (isopropylcyclopentadienyl) lanthanum (La(ⁱPrCp)₃) and trimethyl-aluminum (TMA) was used as the lanthanum and aluminum precursor, respectively. H₂O and O₃ was used as the oxidant, respectively. O₃ was generated by the ozone generator using ultra-pure O₂ (99.999%). 10 deposition sequence cycles of TMA/H₂O/La(ⁱPrCp)₃/H₂O and TMA/O₃/La(ⁱPrCp)₃/O₃ were used to obtain H₂O-based La₂O₃/Al₂O₃ nanolaminates and O₃-based La₂O₃/Al₂O₃ nanolaminates, respectively. Before the ALD deposition sequence, a 4 s pulse time of TMA was carried out firstly to form the physical adsorption on the surface. ~3 nm H₂O-based La₂O₃/Al₂O₃ nanolaminates and O₃-based La₂O₃/Al₂O₃ nanolaminates were measured by Woollam M2000D spectroscopic ellipsometry. After O₃-based and H₂O-based La₂O₃/Al₂O₃ nanolaminates deposition process, Al electrode was fabricated by photolithography patterning to form MOS capacitors after back Al electrode was prepared by magnetron sputtering. Atomic force microscopy (AFM, Bruker Dimension Edge, Bruker Nano Inc., Billerica, WA, USA), X-ray photoelectron spectroscopy (XPS, Thermo Scientific K-Alpha, Thermo Fisher Scientific Inc., Waltham, MA, USA) were used to character the properties of La₂O₃/Al₂O₃ nanolaminates on MoS₂. The standard electrical measurements were performed at room temperature using the Keithley 4200SCS characterization system (Tektronix Inc., Kent, WA, USA).

3. Results and Discussion

Figure 2 shows the AFM results of La₂O₃/Al₂O₃ nanolaminates on MoS₂. It can be found that non-uniformity surface is observed for both O₃-based and H₂O-based La₂O₃/Al₂O₃ nanolaminates on MoS₂, which indicates that it is difficult to grow uniform ultrathin dielectric directly on MoS₂. Meanwhile, a smoother surface is obtained for O₃-based La₂O₃/Al₂O₃ nanolaminates compared to H₂O-based La₂O₃/Al₂O₃ nanolaminates on MoS₂. This may be explained by that, O₃ has higher reactivity due to its strong oxidizing ability, it is easy to decompose to O₂ and monatomic O during the ALD reactions, the monatomic O radical diffusion and desorption will significantly affect the growth of the film. Using ozone as oxidant enhances the Al₂O₃ film coverage and uniformity on MoS₂ due to ozone facilitates initial TMA precursor nucleation on the MoS₂ [20], which is consistent with the AFM results. After MoS₂ treated with UV-O₃, the improvement of the uniform surface is observed for both O₃-based and H₂O-based La₂O₃/Al₂O₃ nanolaminates (and especially for O₃-based La₂O₃/Al₂O₃ nanolaminates). The root mean square (RMS) value of O₃-based La₂O₃/Al₂O₃ nanolaminates decreases from 0.381 nm to 0.150 nm, while the RMS value of H₂O-based La₂O₃/Al₂O₃ nanolaminates decreases from 0.394 nm to 0.186 nm after MoS₂ suffered from UV-O₃ treatment. Generally, the lack of reaction surface for MoS₂ lead to an increase of surface roughness after ALD deposition due to the buildup of precursors and reaction products randomly occurred [11]. The improvement of uniform and decrease of RMS value suggest that the initial surface nucleation of ultrathin La₂O₃/Al₂O₃ nanolaminates on MoS₂ can be improved by UV-O₃ treatment.

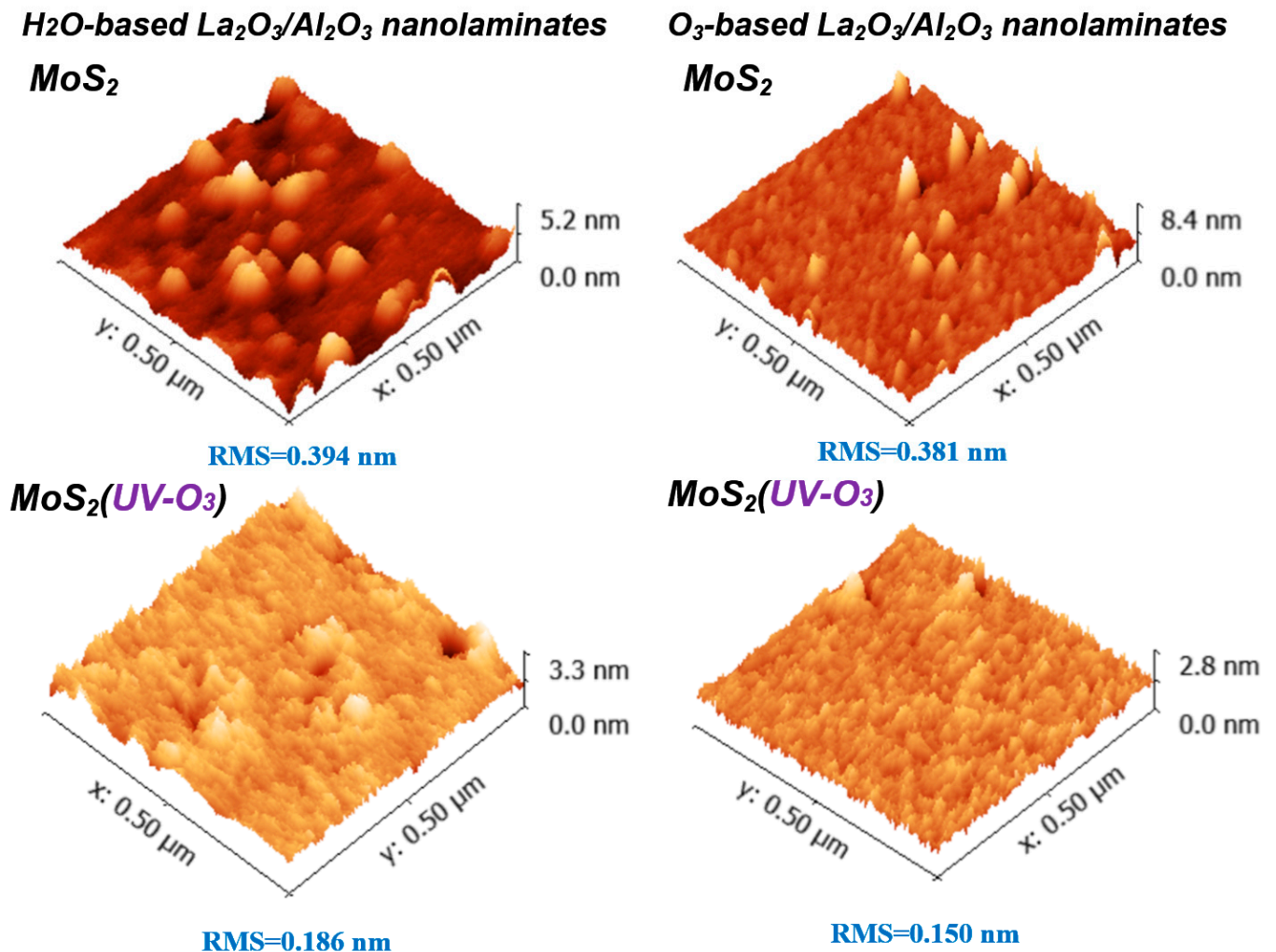


Figure 2. AFM results of sub-5 nm $\text{La}_2\text{O}_3/\text{Al}_2\text{O}_3$ nanolaminates on MoS_2 with or without UV-O_3 treatment.

To evaluate the dielectric electrical properties with nanometer resolution, conductive AFM measurements are carried out by applying a constant voltage between the Pt-Ir coated tip and sample. Figure 3 shows the current images measured by conductive AFM when applying a sample bias of 1 V. As shown in Figure 3, the density of leakage dots in the H_2O -based $\text{La}_2\text{O}_3/\text{Al}_2\text{O}_3$ nanolaminates is higher than that in the O_3 -based $\text{La}_2\text{O}_3/\text{Al}_2\text{O}_3$ nanolaminates. The leakage dot is an indicator of conductive paths exist in $\text{La}_2\text{O}_3/\text{Al}_2\text{O}_3$ nanolaminates. They are not only attributed to surface roughness, but also possibly caused by local fluctuations in composition and/or structures, and/or by defects in $\text{La}_2\text{O}_3/\text{Al}_2\text{O}_3$ nanolaminates [21]. The presence of many leakage dots indicates that H_2O -based $\text{La}_2\text{O}_3/\text{Al}_2\text{O}_3$ nanolaminates on MoS_2 is not suitable for use as a gate dielectric layer. After MoS_2 treated with UV-O_3 treatment, the leakage dots for both O_3 -based and H_2O -based $\text{La}_2\text{O}_3/\text{Al}_2\text{O}_3$ nanolaminates decreased. In particular, no leakage dot is observed for O_3 -based $\text{La}_2\text{O}_3/\text{Al}_2\text{O}_3$ nanolaminates. It indicates that, with the help of UV-O_3 treatment, ultrathin O_3 -based $\text{La}_2\text{O}_3/\text{Al}_2\text{O}_3$ nanolaminates on MoS_2 can serve as the gate dielectric due to its good leakage suppression properties.

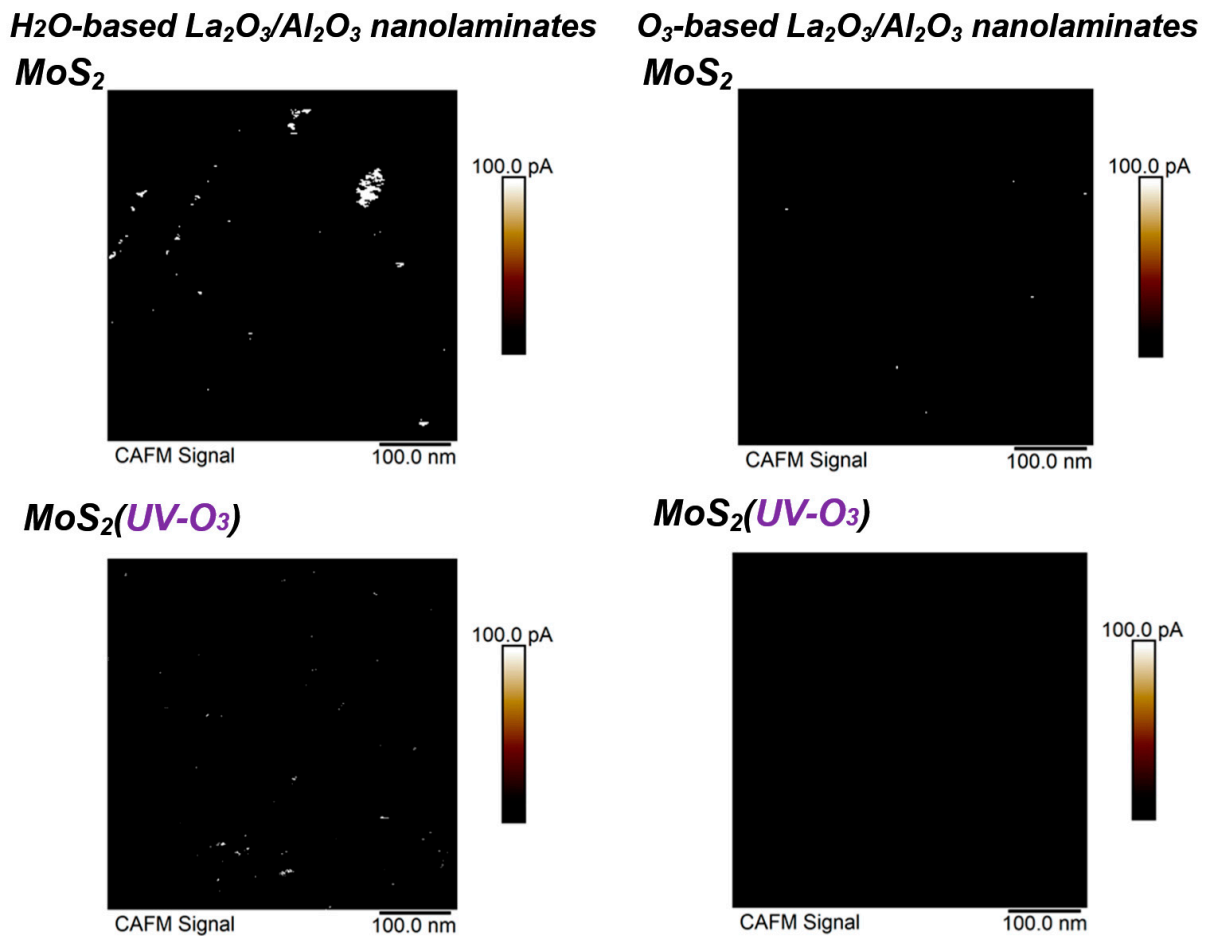


Figure 3. Conductive AFM images of sub-5 nm $\text{La}_2\text{O}_3/\text{Al}_2\text{O}_3$ nanolaminates on MoS_2 with or without UV-O_3 treatment.

The changes in uniformity of $\text{La}_2\text{O}_3/\text{Al}_2\text{O}_3$ nanolaminates on MoS_2 may be originated from the interface due to the ALD process of growing $\text{La}_2\text{O}_3/\text{Al}_2\text{O}_3$ nanolaminates on silicon is well established [17]. To reveal the changes that occurred at the interface, XPS measurements are performed. Figure 4 shows the C_{1s} spectra of $\text{La}_2\text{O}_3/\text{Al}_2\text{O}_3$ nanolaminates on MoS_2 . There are mainly two peaks in the C_{1s} spectra for all $\text{La}_2\text{O}_3/\text{Al}_2\text{O}_3$ nanolaminates on MoS_2 , which are located at binding energies of 283.0 eV and 284.8 eV. These peaks correspond to the metal carbide and adsorbed carbon, respectively [22]. Moreover, the peak intensity of metal carbide in H_2O -based ALD process decreases from 30.0 a.t.% to 15.8 a.t.% after MoS_2 suffered from UV-O_3 treatment, while that of O_3 -based ALD process decreases from 11.9 a.t.% to 9.8 a.t.%. The lowest metal carbide content in O_3 -based $\text{La}_2\text{O}_3/\text{Al}_2\text{O}_3$ nanolaminates on MoS_2 with UV-O_3 treatment suggests that the initial interfacial reactions are greatly improved. The appearance of metal carbide is an indication that poor interface reactions occur during the ALD process, which can originate from the generation of intermediates or by-products of metal precursors. MoS_2 suffered from low-power UV-O_3 treatment form the weak chemical bond of S-O on the surface without hampering its electrical performance [15], which can supply the reaction interface groups at the MoS_2 surface during the ALD deposition. As a result, the residuals of the metal carbide or its intermediate precursor during the first ALD reaction cycles can be reduced and the roughness of the nanolaminates can be improved.

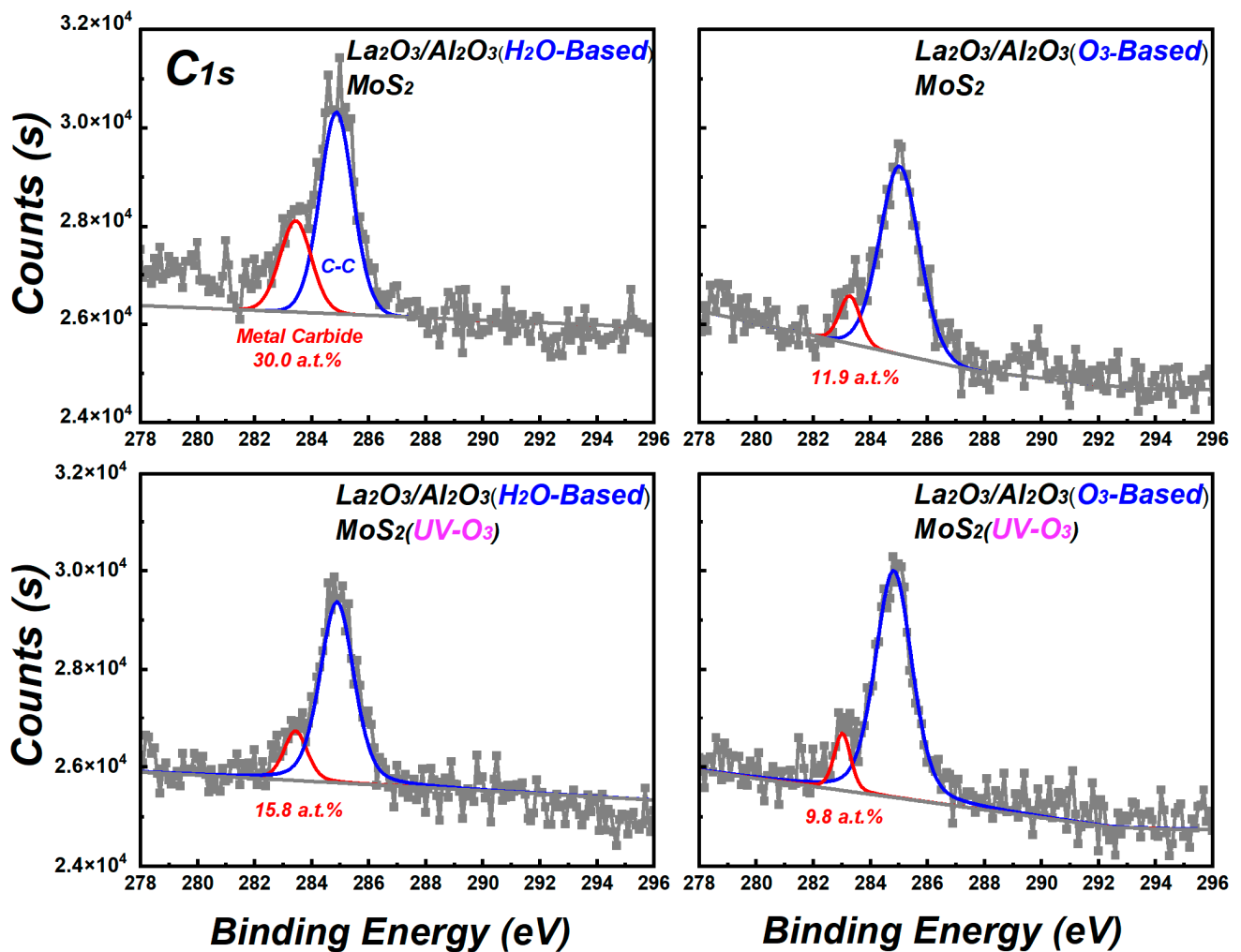


Figure 4. C_{1s} spectra of La₂O₃/Al₂O₃ nanolaminates on MoS₂.

In order to further confirm the residue in La₂O₃/Al₂O₃ nanolaminates on MoS₂, Figure 5 shows the Al_{2p} spectra of La₂O₃/Al₂O₃ nanolaminates on MoS₂. As shown in Figure 5, the Al_{2p} spectra can be fitted to two peaks, which located at the binding energy of ~74.6 eV and 73.8 eV, respectively. 74.6 eV belongs to the Al-O bond, and the lower 73.8 eV is related to carbide [22]. The content of carbide in H₂O-based La₂O₃/Al₂O₃ nanolaminates decreases from 9.66 a.t.% to 3.88 a.t.% after MoS₂ treated with UV-O₃ treatment, while that of O₃-based La₂O₃/Al₂O₃ nanolaminates decreases from 2.98 a.t.% to 0.92 a.t.% after MoS₂ treated with UV-O₃ treatment. The variation of carbide content in La₂O₃/Al₂O₃ nanolaminates on MoS₂ is consistent with the C_{1s} results. Due to lack of dangling bonds or nucleation sites on MoS₂, the initial reaction of ALD is dependent on weakly physical adsorbed TMA precursors on MoS₂ surface. UV-O₃ treatment forms the weak S-O bonds on MoS₂ and facilitates the uniform physical adsorption of precursor, which is beneficial for the improvement of initial ALD self-limiting surface reactions. O₃ has a stronger ability than water to split the C-H or Al-C bonds which attached to metal atoms in the deposition [18]. As a result, the concentration of metal carbide in O₃-based La₂O₃/Al₂O₃ nanolaminates is lower than H₂O-based La₂O₃/Al₂O₃ nanolaminates.

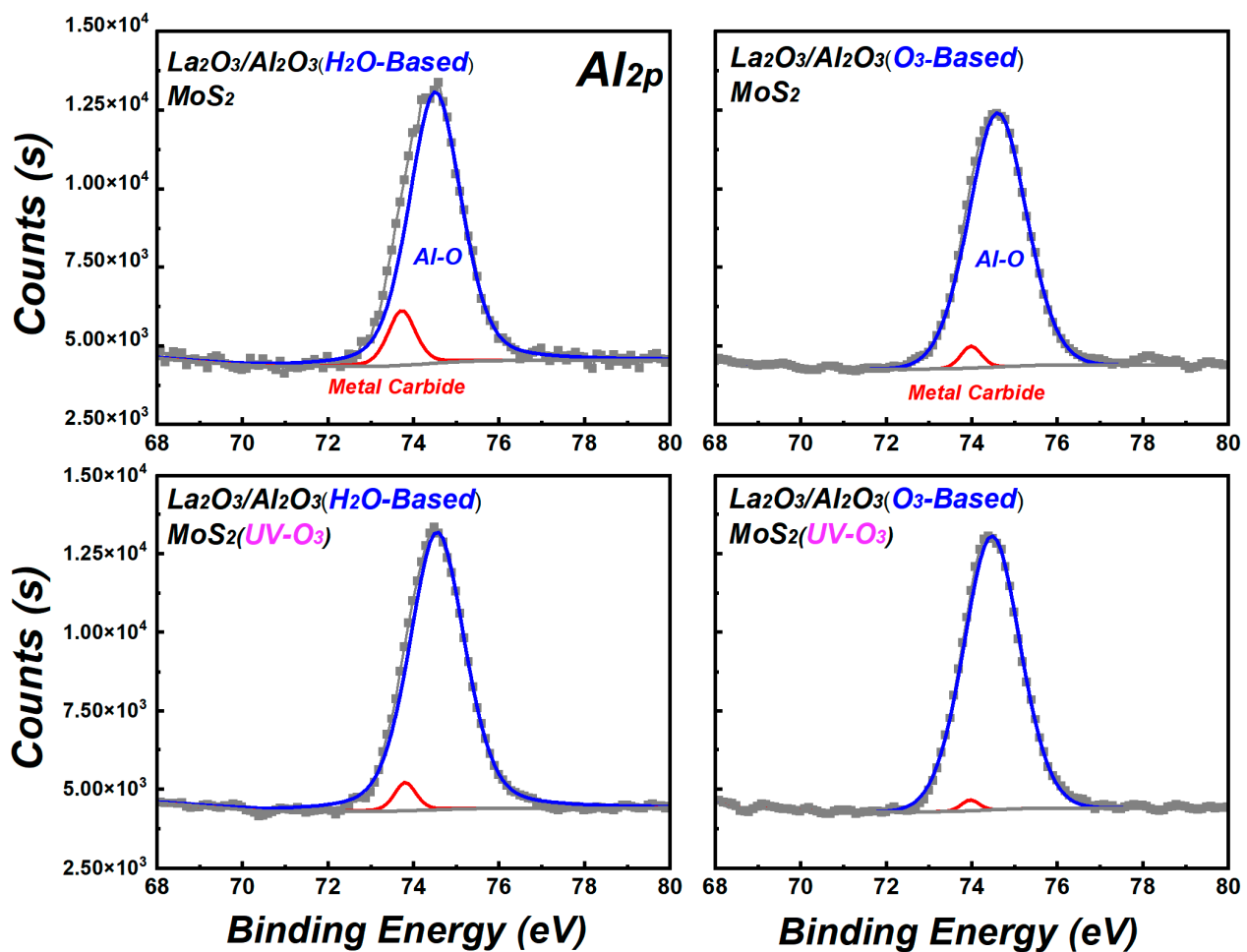


Figure 5. Al_{2p} spectra of La_2O_3/Al_2O_3 nanolaminates on MoS_2 .

To determine the valence band offset (VBO) between La_2O_3/Al_2O_3 nanolaminates and MoS_2 , the Kraut method is used which discussed in ref. [23],

$$\Delta E_{VBO} = \left(E_{CL}^{Mo_{3p}} - E_V \right)_{bulk, MoS_2} - \left(E_{CL}^{Al_{2p}} - E_V \right)_{thick\ nanolaminates} - \left(E_{CL}^{Mo_{3p}} - E_{CL}^{Al_{2p}} \right)_{thin\ nanolaminates/MoS_2} \quad (1)$$

where $E_{CL}^{Mo_{3p}}$ and $E_{CL}^{Al_{2p}}$ is the binding energy of the Mo_{3p} and Al_{2p} shallow core levels, respectively. E_V is the binding energy corresponding to the valence band maximum (VBM). The value of VBM is determined by the intercept of the slope at the leading edge of the valence band spectrum with the base line. To correct the differential charging, the binding energy calibration was performed using a gold standard sample. Figure 6 shows the core level spectra of ~10 nm sputtered MoS_2 with or without UV- O_3 treatment. The energy difference between the Mo_{3p} core level and the VBM is 394.58 eV and 394.59 eV for the clean MoS_2 and MoS_2 treated with UV- O_3 treatment, respectively. These values are agreed well with the values reported in ref. [24].

Figure 7 shows the XPS core level spectra of Mo_{3p} and Al_{2p} for La_2O_3/Al_2O_3 nanolaminates. The core level energies are obtained by curve fitting to ensure high accuracy binding energy of the peak. In order to measure the band offset between La_2O_3/Al_2O_3 nanolaminates and MoS_2 , ~10 nm H_2O -based and O_3 -based La_2O_3/Al_2O_3 nanolaminates are prepared for use as bulk films, respectively. As shown in Figure 7, the energy difference values between the core level energies are determined. Using these energy difference values with Equation (1), the VBO values of the H_2O -based and O_3 -based La_2O_3/Al_2O_3 nanolaminates on MoS_2 can be derived. The VBO of 3.10 eV and 3.14 eV is obtained for O_3 -based La_2O_3/Al_2O_3 nanolaminates on MoS_2 and MoS_2 with UV- O_3 treatment, respec-

tively. In addition, the VBO of H₂O-based nanolaminates on MoS₂ and MoS₂ with UV-O₃ treatment is 2.75 eV and 2.91 eV, respectively. The results indicate that the VBO is affected by the different oxidants and UV-O₃ treatment. The negligible VBO variations for O₃-based La₂O₃/Al₂O₃ nanolaminates suggest that it has a better stability compared to H₂O-based La₂O₃/Al₂O₃ nanolaminates.

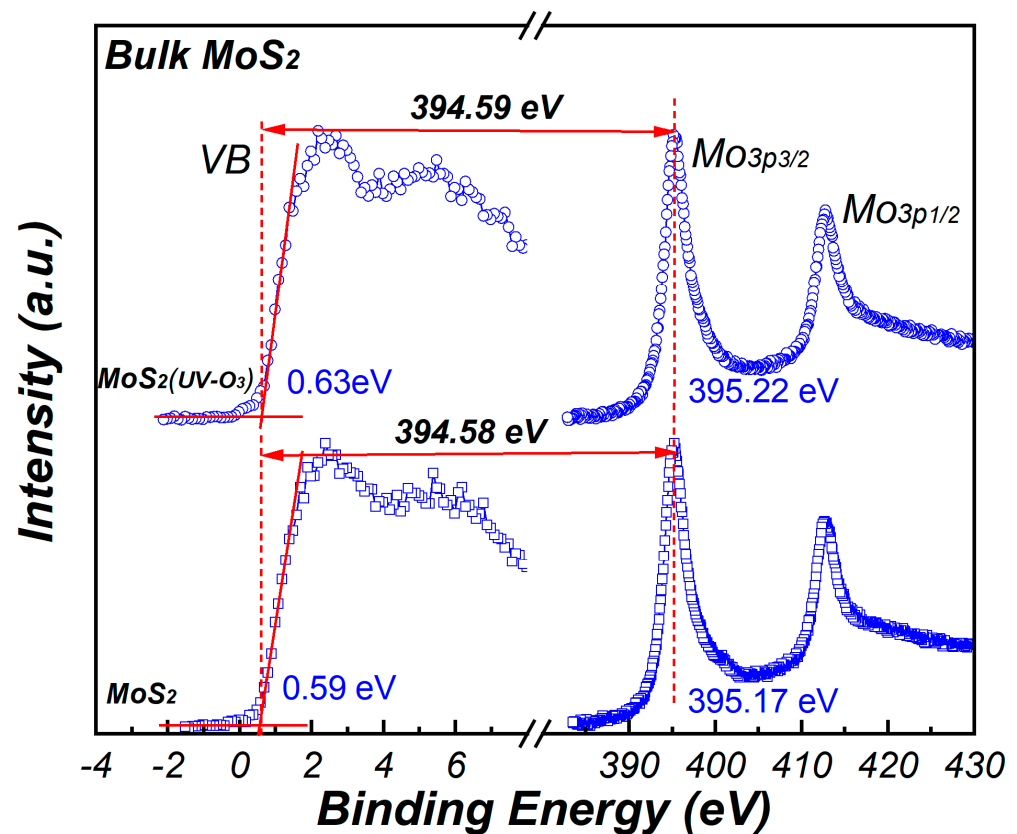


Figure 6. The XPS core level spectra of Mo_{3p} for MoS₂.

To obtain the conduction band offset (CBO) between La₂O₃/Al₂O₃ nanolaminates and MoS₂, the optical band gaps of La₂O₃/Al₂O₃ nanolaminates are measured. The optical band gaps from the plots of $(\alpha E)^2$ versus photo energy E are shown in Figure 8. The extrapolation of the linear part of $(\alpha E)^2 - E$ down to $(\alpha E)^2 = 0$ gives the values of band gaps [25]. The measured band gap value of O₃-based and H₂O-based La₂O₃/Al₂O₃ nanolaminates is 6.37 eV and 6.19 eV, respectively. These values are in good agreement with the reported values of La₂O₃/Al₂O₃ gate stack or LaAlO₃ films ranging from 6.1–6.4 eV [17,26]. The results indicate that the O₃-based La₂O₃/Al₂O₃ nanolaminates has a larger bandgap value compared to the H₂O-based nanolaminates. This may be caused by the lower content of impurities found in O₃-based La₂O₃/Al₂O₃ nanolaminates compared to H₂O-based nanolaminates.

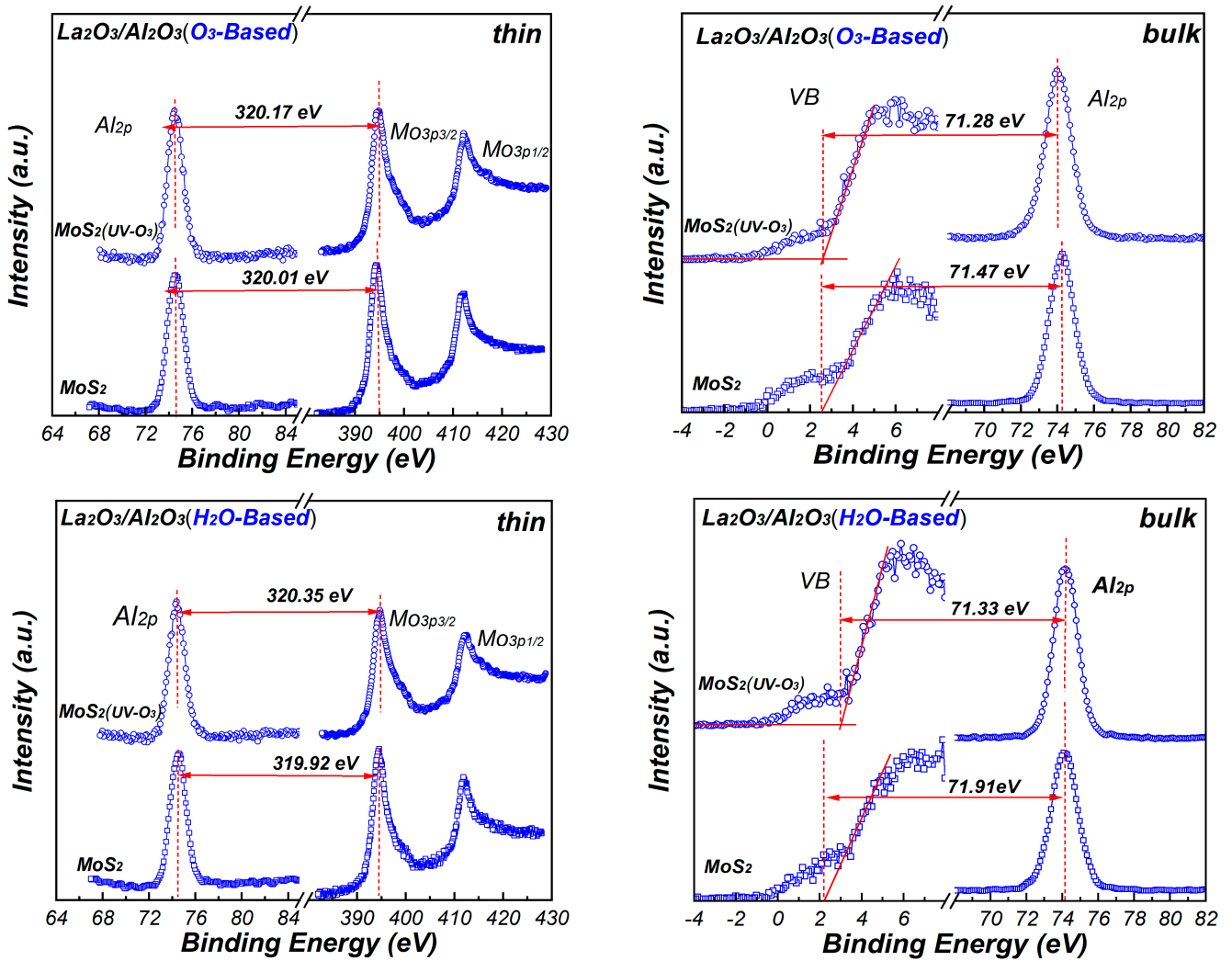


Figure 7. The XPS core-level and valence band spectra of thin and bulk $\text{La}_2\text{O}_3/\text{Al}_2\text{O}_3$ nanolaminates.

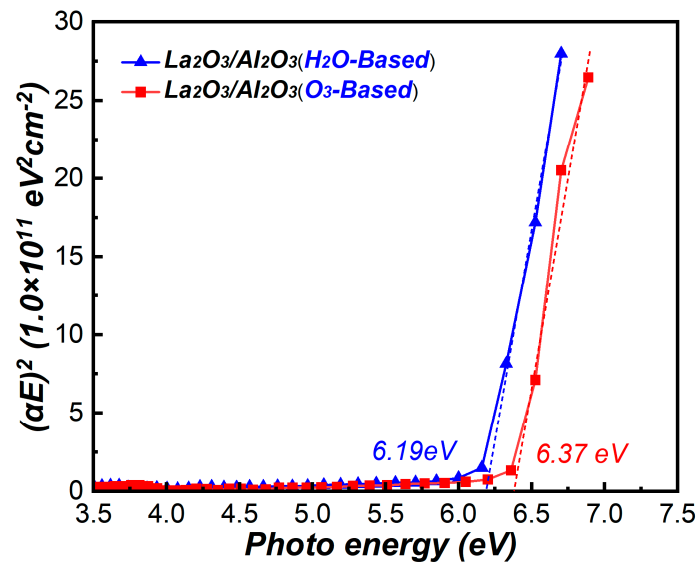


Figure 8. $(\alpha E)^2$ versus photo energy E of $\text{La}_2\text{O}_3/\text{Al}_2\text{O}_3$ nanolaminates.

Using the calculated VBO and band gap values, the conduction band offset between $\text{La}_2\text{O}_3/\text{Al}_2\text{O}_3$ nanolaminates and MoS_2 can be attained by the following equation:

$$\Delta E_{CBO} = E_g^{\text{La}_2\text{O}_3/\text{Al}_2\text{O}_3 \text{ nanolaminates}} - E_g^{\text{MoS}_2} - \Delta E_{VBO} \quad (2)$$

where $E_g^{\text{La}_2\text{O}_3/\text{Al}_2\text{O}_3 \text{ nanolaminates}}$ and $E_g^{\text{MoS}_2}$ is the bandgap of $\text{La}_2\text{O}_3/\text{Al}_2\text{O}_3$ nanolaminates and MoS_2 , respectively. The bandgap of 1.4 eV for MoS_2 is used here [27]. According to the Equation (2), the CBO of O_3 -based $\text{La}_2\text{O}_3/\text{Al}_2\text{O}_3$ nanolaminates on MoS_2 and MoS_2 with UV- O_3 treatment is 1.87 eV and 1.83 eV, respectively. Meanwhile, the CBO of H_2O -based $\text{La}_2\text{O}_3/\text{Al}_2\text{O}_3$ nanolaminates on MoS_2 and MoS_2 with UV- O_3 treatment is 2.04 eV and 1.88 eV, respectively. The corresponding band diagrams are illustrated in Figure 9. It can be seen that both $\text{La}_2\text{O}_3/\text{Al}_2\text{O}_3$ nanolaminates/ MoS_2 interface have a Type I alignment, where the conduction band edge and valence band edge of MoS_2 are located within the bandgap of $\text{La}_2\text{O}_3/\text{Al}_2\text{O}_3$ nanolaminates. Furthermore, both CBO and VBO values of $\text{La}_2\text{O}_3/\text{Al}_2\text{O}_3$ nanolaminates on MoS_2 provide excellent electron and hole barriers due to their values larger than 1 eV, ensuring $\text{La}_2\text{O}_3/\text{Al}_2\text{O}_3$ nanolaminates suitability for FETs applications. Remarkably, O_3 -based $\text{La}_2\text{O}_3/\text{Al}_2\text{O}_3$ nanolaminates has a higher VBO compare with H_2O -based $\text{La}_2\text{O}_3/\text{Al}_2\text{O}_3$ nanolaminates, which is better for p -channel FETs application.

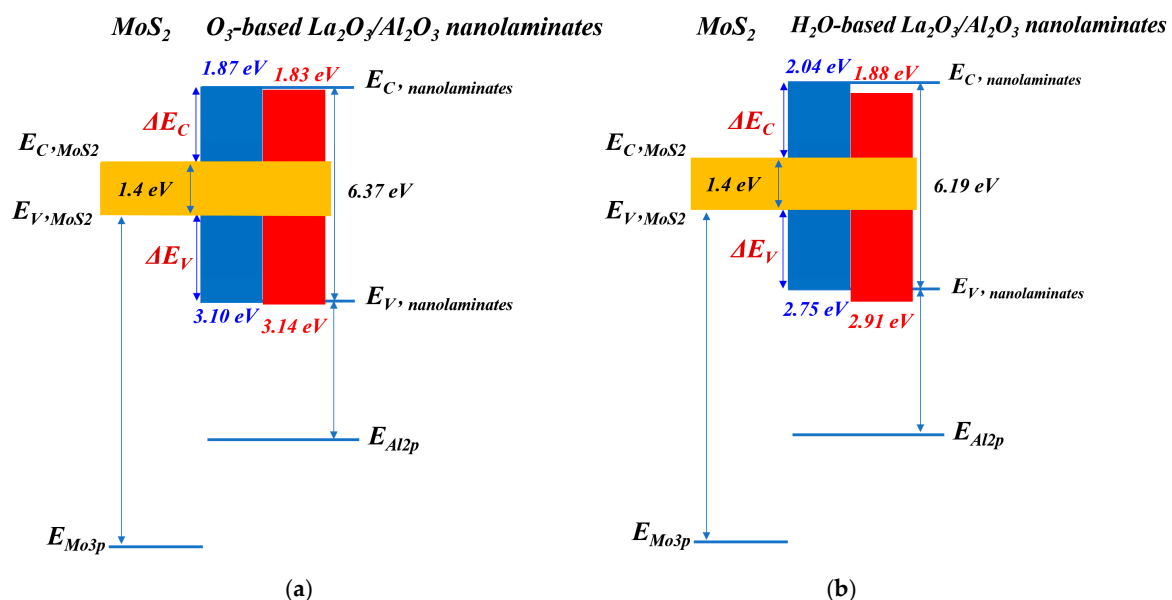


Figure 9. Band diagrams of (a) O_3 -based $\text{La}_2\text{O}_3/\text{Al}_2\text{O}_3$ nanolaminates and (b) H_2O -based $\text{La}_2\text{O}_3/\text{Al}_2\text{O}_3$ nanolaminates on MoS_2 (Blue for MoS_2 and red for MoS_2 treated with UV- O_3 treatment).

Figure 10 shows the I-V curves of $\text{La}_2\text{O}_3/\text{Al}_2\text{O}_3$ nanolaminates on MoS_2 after fabricated metal-oxide-semiconductor (MOS) capacitor. At the applied voltage of 2 V, for O_3 -based $\text{La}_2\text{O}_3/\text{Al}_2\text{O}_3$ nanolaminates, the leakage current decreased from 1.2×10^{-2} mA to 9.6×10^{-3} mA, while the breakdown voltage increased from 9.01 V to 10.21 V after MoS_2 treated with UV- O_3 treatment. The same trend is observed in H_2O -based $\text{La}_2\text{O}_3/\text{Al}_2\text{O}_3$ nanolaminates. The leakage current decreased from 2.6×10^{-2} mA to 2.3×10^{-2} mA, while the breakdown voltage increased from 6.76 V to 7.36 V after MoS_2 treated with UV- O_3 treatment. The breakdown voltage is obtained when the leakage current reaches 1 mA [28]. The decrease of leakage current and increase of breakdown voltage may be attributed to the uniformity of the $\text{La}_2\text{O}_3/\text{Al}_2\text{O}_3$ nanolaminates as well as the reduction of impurities or residuals at the interface. The leakage current may originate either Poole-Frenkel or Fowler-Nordheim mechanism from the point of view of quantum tunneling [29,30], which has been confirmed in our measurement. The lowest leakage current and highest break-

down voltage are obtained for O₃-based La₂O₃/Al₂O₃ nanolaminates on MoS₂ with UV-O₃ treatment, making it a promising dielectric candidate for the application of MoS₂ FETs.

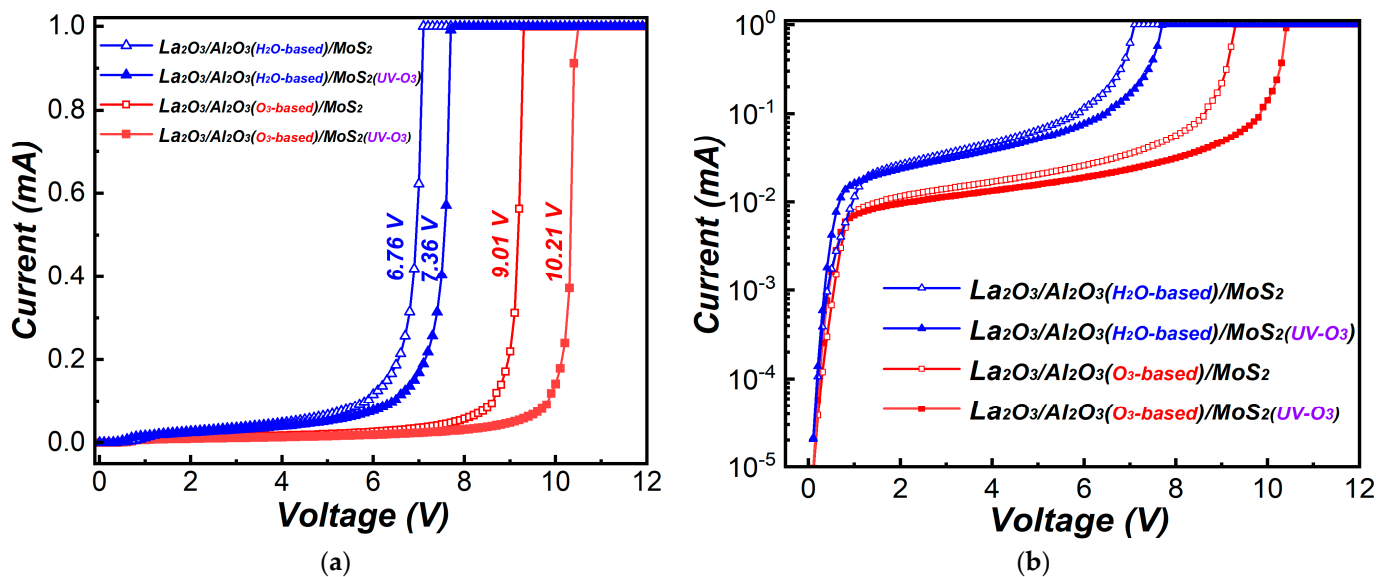


Figure 10. (a) Linear-scale and (b) log-scale I-V curves of MOS capacitors for La₂O₃/Al₂O₃ nanolaminates on MoS₂.

4. Conclusions

In this study, atomic layer deposition growth of sub-5 nm La₂O₃/Al₂O₃ nanolaminates on MoS₂ using different oxidants (H₂O and O₃) and the UV-O₃ pretreatment on MoS₂ are investigated. Compared with H₂O-based La₂O₃/Al₂O₃ nanolaminates on MoS₂, better uniformity and lower leakage dots were observed for O₃-based La₂O₃/Al₂O₃ nanolaminates on MoS₂. This is associated with the metal carbide concentration in La₂O₃/Al₂O₃ nanolaminates on MoS₂, which is generated by insufficient interfacial reactions. UV-O₃ treatment can decrease the residuals of the metal carbide and improve the deposition of La₂O₃/Al₂O₃ nanolaminates on the MoS₂ interface by introducing the weak S-O bonds to MoS₂ surface, leading to the properties of La₂O₃/Al₂O₃ nanolaminates being substantially improved. The band offset values of both O₃-based and H₂O-based La₂O₃/Al₂O₃ nanolaminates/MoS₂ are larger than 1 eV, which can provide eligible electron and hole barrier height. In particular, a higher valence band offset is obtained for O₃-based La₂O₃/Al₂O₃ nanolaminates compared to H₂O-based La₂O₃/Al₂O₃ nanolaminates. Consequently, O₃-based La₂O₃/Al₂O₃ nanolaminates on MoS₂ exhibits smaller leakage current and higher breakdown voltage, especially after MoS₂ suffered from UV-O₃ treatment. All results indicate that O₃-based La₂O₃/Al₂O₃ nanolaminates on MoS₂ with UV-O₃ treatment is a more appropriate process to obtain sub-5 nm uniform La₂O₃/Al₂O₃ nanolaminates on MoS₂ due to its good electrical characteristics, providing important implications for its integration into transistors.

Author Contributions: J.F. performed the data analyses and wrote the manuscript; Y.S., performed the experiment; H.L., S.W. and L.D. helped perform the analysis with constructive discussions; L.L., Y.Z. and X.W. contributed to the conception of the study. All authors have read and agreed to the published version of the manuscript.

Funding: This work was supported by the National Natural Science Foundation of China (Grant Nos. 61604016, 51501017 and 51802025), China Postdoctoral Science Foundation (Grant No. 2017M613028), Natural Science Foundation of Shaanxi Province, China (2021GY-255), the Fundamental Research Funds for the Central Universities (Grant No. 300102319209).

Institutional Review Board Statement: Not applicable.

Informed Consent Statement: Not applicable.

Data Availability Statement: Data will be made available upon reasonable request.

Conflicts of Interest: The authors declare no conflict of interest.

References

1. Maurand, R.; Jehl, X.; Kotekar-Patil, D.; Corna, A.; Bohuslavskiy, H.; Laviéville, R.; Hutin, L.; Barraud, S.; Vinet, M.; Sanquer, M.; et al. A CMOS silicon spin qubit. *Nat. Commun.* **2016**, *7*, 13575. [[CrossRef](#)] [[PubMed](#)]
2. Auth, C.; Aliyarukunju, A.; Asoro, M.; Bergstrom, D.; Bhagwat, V.; Birdsall, J.; Bisnik, N.; Buehler, M.; Chikarmane, V.; Ding, G.; et al. A 10 nm High Performance and Low-Power CMOS Technology Featuring 3rd Generation FinFET Transistors, Self-Aligned Quad Patterning, Contact over Active Gate and Cobalt Local Interconnects. In Proceedings of the 2017 IEEE International Electron Devices Meeting (IEDM), San Francisco, CA, USA, 2–6 December 2017; pp. 29.21.21–29.21.24.
3. Gong, C.; Zhang, Y.; Chen, W.; Chu, J.; Lei, T.; Pu, J.; Dai, L.; Wu, C.; Cheng, Y.; Zhai, T.; et al. Electronic and Optoelectronic Applications Based on 2D Novel Anisotropic Transition Metal Dichalcogenides. *Adv. Sci.* **2017**, *4*, 1700231. [[CrossRef](#)]
4. Samadi, M.; Sarikhani, N.; Zirak, M.; Zhang, H.; Zhang, H.-L.; Moshfegh, A.Z. Group 6 transition metal dichalcogenide nanomaterials: Synthesis, applications and future perspectives. *Nanoscale Horiz.* **2017**, *3*, 90–204. [[CrossRef](#)] [[PubMed](#)]
5. Nourbakhsh, A.; Zubair, A.; Sajjad, R.N.; Amir Tavakkoli, K.G.; Chen, W.; Fang, S.; Ling, X.; Kong, J.; Dresselhaus, M.S.; Kaxiras, E.; et al. MoS₂ Field-Effect Transistor with Sub-10 nm Channel Length. *Nano Lett.* **2016**, *16*, 7798–7806. [[CrossRef](#)] [[PubMed](#)]
6. Singh, E.; Singh, P.; Kim, K.; Yeom, G.Y.; Nalwa, H.S. Flexible molybdenum disulfide (MoS₂) atomic layers for wearable electronics and optoelectronics. *ACS Appl. Mater. Interfaces* **2019**, *11*, 11061–11105. [[CrossRef](#)]
7. Li, W.; Zhou, J.; Cai, S.; Yu, Z.; Zhang, J.; Fang, N.; Li, T.; Wu, Y.; Chen, T.; Xie, X.; et al. Uniform and ultrathin high- κ gate dielectrics for two-dimensional electronic devices. *Nat. Electron.* **2019**, *2*, 563–571. [[CrossRef](#)]
8. Joo, M.; Yun, Y.; Ji, H.; Suh, D. Coulomb scattering mechanism transition in 2D layered MoTe₂: Effect of high-kappa passivation and Schottky barrier height. *Nanotechnology* **2019**, *30*, 035206. [[CrossRef](#)]
9. Li, N.; Wei, Z.; Zhao, J.; Wang, Q.; Shen, C.; Wang, S.; Tang, J.; Yang, R.; Shi, D.; Zhang, G. Atomic Layer Deposition of Al₂O₃ Directly on 2D Materials for High-Performance Electronics. *Adv. Mater. Interfaces* **2019**, *6*, 1802055. [[CrossRef](#)]
10. Park, T.; Kim, H.; Leem, M.; Ahn, W.; Choi, S.; Kim, J.; Uh, J.; Kwon, K.; Jeong, S.-J.; Park, S.; et al. Atomic Layer Deposition of Al₂O₃ on MoS₂, WS₂, WSe₂, and *h*-BN: Surface Coverage and Adsorption Energy. *RSC Adv.* **2017**, *7*, 884–889. [[CrossRef](#)]
11. Kim, H.G.; Lee, H. Atomic Layer Deposition on 2D Materials. *Chem. Mater.* **2017**, *9*, 3809–3826. [[CrossRef](#)]
12. Price, K.M.; Schauble, K.E.; McGuire, F.A.; Farmer, D.B.; Franklin, A.D. Uniform Growth of Sub-5-Nanometer High- κ Dielectrics on MoS₂ Using Plasma-Enhanced Atomic Layer Deposition. *ACS Appl. Mater. Interfaces* **2017**, *9*, 23072–23080. [[CrossRef](#)]
13. Yang, J.; Kim, S.; Choi, W.; Park, S.H.; Jung, Y.; Cho, M.H.; Kim, H. Improved growth behavior of atomic-layer-deposited high- κ dielectrics on multilayer MoS₂ by oxygen plasma pretreatment. *ACS Appl. Mater. Interfaces* **2013**, *5*, 4739–4744. [[CrossRef](#)] [[PubMed](#)]
14. Zhang, H.; Arutchelvan, G.; Meersschant, J.; Gaur, A.; Conard, T.; Bender, H.; Lin, D. MoS₂ functionalization with a sub-nm thin SiO₂ layer for atomic layer deposition of high- κ dielectrics. *Chem. Mater.* **2017**, *29*, 6772–6780. [[CrossRef](#)]
15. Park, S.; Kim, S.Y.; Choi, Y.; Kim, M.; Shin, H.; Kim, J.; Choi, W. Interface properties of atomic-layer-deposited Al₂O₃ thin films on Ultraviolet/Ozone-treated multilayer MoS₂ crystals. *ACS Appl. Mater. Interfaces* **2016**, *8*, 11189–11193. [[CrossRef](#)] [[PubMed](#)]
16. Huang, B.; Zheng, M.; Zhao, Y.; Wu, J.; Thong, J.T.L. Atomic Layer Deposition of High-Quality Al₂O₃ Thin Films on MoS₂ with Water Plasma Treatment. *ACS Appl. Mater. Interfaces* **2019**, *11*, 35438–35443. [[CrossRef](#)]
17. Fujitsuka, R.; Sakashita, M.; Sakai, A.; Ogawa, M.; Zaima, S.; Yasuda, Y. Thermal stability and electrical properties of (La₂O₃)_{1-x}(Al₂O₃)_x composite films. *Jpn. J. Appl. Phys.* **2005**, *44*, 2428–2432. [[CrossRef](#)]
18. Zhao, L.; Liu, H.; Wang, X.; Feng, X.; Fei, C. Band alignments of O₃-based and H₂O-based amorphous LaAlO₃ films on silicon by atomic layer deposition. *J. Mater. Sci. Mater. Electron.* **2017**, *28*, 803–807. [[CrossRef](#)]
19. Singh, R.; Tripathi, S. Structural and optical properties of few-layer MoS₂ thin films grown on various substrates using RF sputtering process. *J. Mater. Sci. Mater. Electron.* **2019**, *30*, 7665–7680. [[CrossRef](#)]
20. Cheng, L.; Qin, X.; Lucero, A.T.; Azcatl, A.; Huang, J.; Wallace, R.M.; Cho, K.; Kim, J. Atomic Layer Deposition of a High- κ Dielectric on MoS₂ Using Trimethylaluminum and Ozone. *ACS Appl. Mater. Interfaces* **2014**, *6*, 11834–11838. [[CrossRef](#)]
21. Iglesias, V.; Wu, Q.; Porti, M.; Nafria, M.; Bersuker, G.; Cordes, A. Monitoring defects in III–V materials: A nanoscale CAFM study. *Microelectron. Eng.* **2015**, *147*, 31–36. [[CrossRef](#)]
22. Xiang, J.; Ding, Y.; Du, L.; Xu, C.; Li, T.; Wang, X.; Li, J.; Zhao, C. Investigation of N Type Metal TiAlC by Thermal Atomic Layer Deposition Using TiCl₄ and TEA as Precursors. *ECS J. Solid State Sci. Technol.* **2016**, *5*, P299–P303. [[CrossRef](#)]
23. Kraut, E.A.; Grant, R.W.; Waldrop, J.R.; Kowalczyk, S.P. Semiconductor core-level to valence-band maximum binding-energy differences: Precise determination by x-ray photoelectron spectroscopy. *Phys. Rev. B* **1983**, *28*, 1965–1977. [[CrossRef](#)]
24. Liu, X.; He, J.; Tang, D.; Liu, Q.; Wen, J.; Yu, W.; Lu, Y.; Zhu, D.; Liu, W.; Cao, P.; et al. Band alignment of atomic layer deposited high- κ Al₂O₃/multilayer MoS₂ interface determined by X-ray photoelectron spectroscopy. *J. Alloys Compd.* **2015**, *650*, 502–507. [[CrossRef](#)]
25. Qasrawi, A.F.; Gasanly, N.M. Refractive index, static dielectric constant, energy band gap and oscillator parameters of Ga₂SeS single crystals. *Phys. Status Solidi* **2007**, *204*, 3165–3169. [[CrossRef](#)]

26. Pelloquin, S.; Saintgiron, G.; Baboux, N.; Albertini, D.; Hourani, W.; Penuelas, J.; Grenet, G.; Plossu, C.; Hollinger, G. LaAlO₃/Si capacitors: Comparison of different molecular beam deposition conditions and their impact on electrical properties. *J. Appl. Phys.* **2013**, *113*, 247–250. [[CrossRef](#)]
27. Mak, K.F.; Lee, C.; Hone, J.; Shan, J.; Heinz, T.F. Atomically thin MoS₂: A new direct-gap semiconductor. *Phys. Rev. Lett.* **2010**, *105*, 136805. [[CrossRef](#)] [[PubMed](#)]
28. Ravariu, C. Vacuum Nano-Triode in Nothing-On-Insulator Configuration Working in Terahertz Domain. *IEEE J. Electron Devices Soc.* **2018**, *6*, 1115–1123. [[CrossRef](#)]
29. Codreanu, C.; Vasile, E.; Iliescu, E.; Avram, M.; Badoiu, A.; Ravariu, C. Free carrier lifetime reduction in silicon by electron-beam irradiation. In Proceedings of the 2000 International Semiconductor Conference. 23rd Edition, Sinaia, Romania, 10–14 October 2000; pp. 255–258.
30. Liu, J.-M.; Shi, G.; Yu, L.; Li, T.; Liu, Z.; Dai, J. Pulsed laser deposition of aluminate YAlO₃ and LaAlO₃ thin films for alternative gate dielectric applications. *Appl. Phys. A* **2005**, *80*, 1775–1779. [[CrossRef](#)]